Asian Journal of Chemistry; Vol. 33, No. 3 (2021), 591-599

ASIAN JOURNAL OF CHEMISTRY

https://doi.org/10.14233/ajchem.2021.23043

Effect of Some Modifier Ions in CuO Doped Sodium Borosilicate Antibacterial Bioglass

Y. SUDHAKAR[1,2], G. SAHAYA BASKARAN[1,*], P. SYAM PRASAD[3], D. RAJESWARA RAO[1] and G. LITTLE FLOWER[4]

[1]Department of Physics, Andhra Loyola College, Vijayawada-520008, India
[2]Department of Physics, Acharya Nagarjuna University, Nagarjuna Nagar-522510, India
[3]Department of Physics, National Institute of Technology, Warangal-506004, India
[4]Department of Physics, Maris Stella College, Vijayawada-520008, India

*Corresponding author: E-mail: sbalc@rediffmail.com

Received: 27 October 2020; *Accepted*: 9 January 2021; *Published online*: 16 February 2021; AJC-20254

A set of sodium borosilicate glasses mixed with different modifier oxides, *viz.*, Li_2O, MgO, CaO and ZnO, doped with antimicrobial oxide *viz.* CuO were synthesized. The structural (FT-IR spectroscopy, SEM and XRD) and bioactivity studies of the glasses were carried out before and after 30 days of immersion in simulated body fluid (SBF) under static conditions. Optical absorption spectra of all the glasses exhibited a broad absorption band identified due to $^2B_{1g} \rightarrow {}^2B_{2g}$ octahedral transition of Cu^{2+} ions. Glass microstructure is analyzed using SEM images and XRD patterns to authenticate glass bioactivity (*viz.* to confirm whether there is formation of hydroxyapatite (HAp) layer on the surface). For further confirmation of the formation of HAp on the surface of the post immerse samples, the FTIR spectra were recorded. The spectra revealed some vibrational peaks of calcium phosphate. Solubility (weight loss due to immersion in SBF) percentage is found to be different for different modifiers mixed glasses containing antibacterial CuO. SEM results confirm apparent nodular calcium phosphate microcrystalites. It is observed that the addition of antimicrobial oxide has a positive effect on the bioactivity of glass and make these glasses as fourth-generation biomaterials, which are being extensively used to heal the wounds in the human body by facilitating the growth of soft tissues.

Keywords: Sodium borosilicate glasses, Hydroxyapatite, Antibacterial glass, Modifier oxides, Simulated body fluid.

INTRODUCTION

Applications of bioglasses in medical fields become innumerable, particularly for wound healing, ulcer treatment and ophthalmology through angiogenesis. Borate glass matrices doped with biologically active bioinorganic ions like copper, cobalt, lithium, gallium, silver, zinc, *etc.*, that act as biochemical cues and accelerate soft tissue regeneration by prompting angiogenesis, osteogenesis and boost bone formation [1-3].

It is expected that Cu^+ and Cu^{2+} are effective in killing bacteria through the generation of reactive oxygen species (ROS), protein oxidation, lipid peroxidation and DNA degradation [4]. Addition of ions of copper (Cu^+ and Cu^{2+}) and cobalt (Co^{2+}) to the bioglasses enhances angiogenesis *in vitro* and *in vivo* [5,6]. Copper ions regulate several factors such as vascular endothelial growth factor (VEGF), fibronectin, angiogenin, collagenase, prostaglandin E-1, ceruloplasmin and FGF1/2 that initiate vasodilation and vascular permeabilization, endothelial cell proliferation, migration and morphogenesis and blood vessel formation through extracellular matrix in angiogenesis therapy [7].

From the molecular point of view, copper induces two signaling pathways in angiogenesis. The first one is owed to copper-activated HIF-1 (hypoxia inducible factor) that initiates angiogenesis [8] and the other is mitogen-activated protein kinase (MAPK) cascades that play a key role in transduction extracellular signals to cellular responses called cell proliferation [9]. It is evident from several earlier reports that copper ions as angiogenic dopants support both hard and soft tissues and hence these ions in combination with bioactive glass become an excellent multifunctional *viz.*, antibacterial, osteoinductive and angiogenic material [10,11].

Antibiotic resistance has become a serious risk to public health. Patients in more than 70% of hospital acquire bacterial

infections, which are resistant to one or more of the traditional antibiotics [12]. The mono and divalent network-modifier ions (*e.g.*, Li^+, Na^+, Ca^{2+} or Mg^{2+}) in the glass involve in ion-exchange process called electrochemical method. Alkali ions leaching increases from lithium to potassium and incorporation of alkaline earth ions (Ca^{2+}, Mg^{2+}) and Zn^{2+}ions in glass system reduces the probability of chemical etching. Certain hydrogen-bearing species, such as H^+, H_3O^+, molecular water (OH^-) or even larger aggregates of the simulated body fluid (SBF) solution are responsible for charge compensation mechanism. Faster healing of wounds is achieved by the release of trace elements such as boron, zinc, silicone, calcium, magnesium, copper, iron and manganese from a bioactive glass [13].

Incorporation of silver, cerium, copper, strontium and zinc ions in glass matrix stimulate antibacterial effects [14-17]. Antibacterial properties of borate ions against Gram-positive and Gram-negative bacterial species make B_2O_3 glasses as a reliable biological and optical glass-forming oxides [18,19]. There is almost no cytotoxicity or inflammation of boron containing bioactive glasses *in vivo*. Calcium, sodium and lithium oxides were integrated in borosilicate glasses individually. However Li^+ ions have been discovered to be great glass modifiers in the non-bridging oxygen locations within borosilicate constructions [20].

Magnesium plays a crucial role in the development, repair and maintenance of human bones by augmenting the proliferation of osteoblasts [21] and facilitates more than three hundred chemical reactions in the human body, the most significant of which is calcium transport control [22,23]. Magnesium and calcium oxides in contrast, function as network modifiers in a silicate glass system, replacing CaO with MgO slowly [24-26].

Lithium is more stable and reactive and is therefore used in several biological processes. The introduction of Li_2O to the borate glass network moves several boron atoms from triangle BO_3 to tetrahedral BO_4 units and adds extra oxygen atoms to the network [27]. Higher bioactive response was demonstrated by lithium-containing bioactive glass samples, points out that the apatite formation is developed by the lithium content [28]. The inclusion of lithium oxide in silicate glasses produces non-bridging oxygen (NBO) and several other structural units of silicate within the glass network [29]. Presence of the OH group shows absorption band at about 3426 cm^{-1} and organic substances peak based about 2963 cm^{-1} in the glasses prepared [30]. Formation of non-bridging oxygen, when boric acid is mixed with glass modifiers such as Li_2CO_3 or other alkali oxides rearranges the internal structure of the glass network [31,32]. Lithium oxide and sodium oxide improve the glass forming ability by increasing oxygen-free bonds leading to decrease of chemical durability and enriching biodegradability.

Like copper, zinc is an important trace mineral well metabolized by humans and exhibits antifungal characteristics. ZnO along with borate glass systems become exceptional materials and attracts attention for many applications. ZnO acts as a network former or modifier. It breaks B–O–B bonds while acting as a network modifier and contributes to the creation of non-bridging oxygen (NBO) ions along with the defects known as strained bonds. ZnO, however, forms the glass network through functional units of ZnO_4, where zinc ions are bonded covalently to four oxygen ions [33-36].

Motivated by these predictions, the present study is aimed to study the influence of some modifier oxides *viz.*, CaO, MgO, Li_2O and ZnO on the bioactivity of sodium borosilicate glass containing small amount of copper oxide.

EXPERIMENTAL

Small amount of copper oxide was doped to sodium borosilicate glass samples and the effect of modifier oxides, *viz.*, Li_2O, MgO, CaO and ZnO were studied. Table-1 shows the chemical compositions (mol%) used for preparation of glasses. The chemical compounds are mechanically mixed and melted in the temperature range 900-950 ºC for 0.5 h in silica crucibles. Other details of the methods adopted for the synthesis of the glass are described previously [37]. The descriptions of the methods adopted and the instruments used for certain measurements (namely, OA spectra and IR spectra) are also mentioned in earlier reports [38,39].

TABLE-1
CHEMICAL COMPOSITION OF THE GLASSES (mol%)

Sample label	B_2O_3	SiO_2	Na_2O	CuO	Modifier oxides (Li_2O/MgO/CaO/ZnO)
LiD	54.5	5	20	0.5	20
MgD	54.5	5	20	0.5	20
CaD	54.5	5	20	0.5	20
ZnD	54.5	5	20	0.5	20

To evaluate, the chemical durability of the samples in simulated body fluid (SBF) solution, weight loss was measured by immersing them in this fluid for different intervals of time. Such measurements were performed by maintaining the ratio of surface area of the sample/volume of the solution as 1:10. The samples were soaked in SBF solution contained in a closed polyethylene bottle and was placed in an incubator at 37 ºC. Interfacial technique (potentiometer) was used by the specific electrodes to determine pH and to track the abundance of ions in the residual solution. The pH value of the leftover physiological fluid was also measured at the periodical intervals.

The SBF solution was prepared according to Kokubo's formula [40] and used to evaluate *in vitr*o bioactivity of the samples in the present study. Description of the concentrations of the different constituents used to prepare the SBF are shown in Table-2. Bioactivity performance of the samples was evaluated by measuring the quantity of apatite deposition when soaked in SBF solution. In the present study, the specimens were completely immersed in SBF solution (at 37 ºC) for a period of 30 days. The quantity of hydroxyapatite (HAp) layer deposited on the surface of the samples was evaluated at different time intervals by measuring variations in the weight of samples and the pH of the residual solution. It may be noted that throughout the study period there was no exchange of the solution. The SEM images of the samples were recorded using Carl Zeiss EVO-MA 15 scanning electron microscope. X-ray diffraction analysis was performed on a PANalytical X'pert Powder X-ray diffractometer).

TABLE-2
CONCENTRATIONS OF IONS IN HUMAN BLOOD PLASMA AND SIMULATED BODY FLUID

Ions	Human blood plasma (mM/L)	Simulated body fluid (c-SBF) (mM/L)
Na^+	142	142
K^+	5	5
Mg^{2+}	1.5	1.5
Ca^{2+}	2.5	2.5
Cl^-	103	147.8
HCO_3^-	27	4.2
HPO_4^{2-}	1	1
SO_4^{2-}	0.5	0.5

RESULTS AND DISCUSSION

UV-visible studies: Strength of the internal augmentation between various structural units in the glass network is reflected by the value of optical band gap. Optical absorption spectra exhibited lowest cut-off wavelength for ZnO mixed glasses, among the four glasses studied (Fig. 1). Additionally, the spectra of all the glasses exhibited a broad absorption band in the spectral region 600-800 nm region. This band is identified due to $^2B_{1g} \rightarrow {}^2B_{2g}$ octahedral transition of Cu^{2+} ions. This band is found to be more intense in the spectrum of Li_2O mixed glasses and the lowest in the spectrum of ZnO mixed glasses. In addition, the spectra of all the glasses have exhibited a weak kink at about 385 nm due to charge transfer from Cu^{2+} ions to Cu^+ ions ($3d^{10} \rightarrow 3d^9 4s^1$). It may be noted here that inspite of the fact, that this transition is spin forbidden, the low symmetry of local electric field in the vicinity of cupric ions makes it possible [41,42]. Moreover, it appears that this band is more intense in the spectrum of ZnO mixed glasses and feeble in the spectrum of Li_2O mixed glasses suggesting more concentration of Cu^{2+} ions were reduced into Cu^+ ions in ZnO mixed glasses. In Li_2O mixed glasses, by and large the copper ions exist in divalent state. The spectra further indicate a gradual reduction of Cu^{2+} ions takes place as modifier Li_2O is successively replaced by MgO, CaO and ZnO. Further, the colour of the glasses mixed with Li_2O was observed to be thick blue while ZnO mixed glasses exhibited a slight green tinge. This observation supports, our argument that copper ions predominantly exist in divalent state in Li_2O mixed glasses and there is a possibility for the existence for a small fraction of these ions in monovalent state in ZnO mixed glasses.

A decrease in the magnitude of optical bands indicates less compactness in the glass network leading to the production of non-bridging oxygen (NBOs) that affects the absorption edge. Table-3 shows the values of energy band gap E_0 and absorption edges for the glasses under investigation.

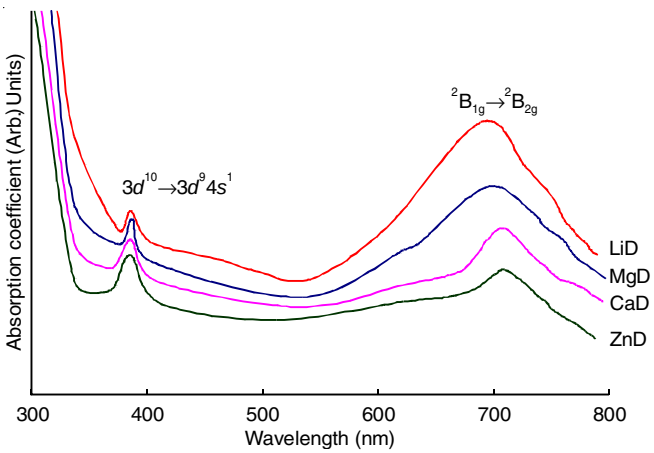

Fig. 1. Optical absorption plots for B_2O_3–SiO_2–Na_2O–CuO:MO glasses

TABLE-3
OPTICAL ABSORPTION DATA OF GLASSES B_2O_3–SiO_2–Na_2O–CuO: MO GLASSES

Glass	Optical band gap E_0 (eV)	Cut-off wavelength (nm)
LiD	2.61	322
MgD	2.72	317
CaD	2.83	308
ZnD	2.97	302

Colour of the glass is an indicator of the ionic environment of the metal ion. The glasses prepared for the present study were blue in colour and formed due to the oxidation states (loss of electrons) of copper ions in Cu^{2+} ($3d^9$, $^2D_{5/2}$ ground state and spin S = ½). To be specific, three bands corresponding to the transitions are predicted for copper ions; $^2B_{1g} \rightarrow {}^2A_{1g}$, $^2B_{1g} \rightarrow {}^2B_{2g}$ and $^2B_{1g} \rightarrow 2E_g$. The OA spectra of CuO doped Li_2O, MgO, CaO and ZnO mixed glasses have exhibited the bands at 385 and 700 nm in the samples of different modifier oxides (Fig. 1). The broad band observed at about 700 nm is due to $^2B_{1g} \rightarrow {}^2B_{2g}$ transition of Cu^{2+} ions situated in tetragonally distorted octahedral sites; this band is found to be more intense in the spectrum of Li_2O mixed glass. The kink observed at low wavelength side is due to the $3d^{10}$ transition of Cu^+ ions. UV-visible spectra of electronic excitation states not only provide the information on valence states of dopant transition metal ions but also give the information on optical band gap E_0 of glasses. The value of E_0 can be evaluated by drawing Tauc plots between $(\alpha h\nu)^{1/2}$ *vs.* hν and by extrapolation of linear portions curves to the hν axis at $(\alpha h\nu)^{1/2}$ as shown in Fig. 2.

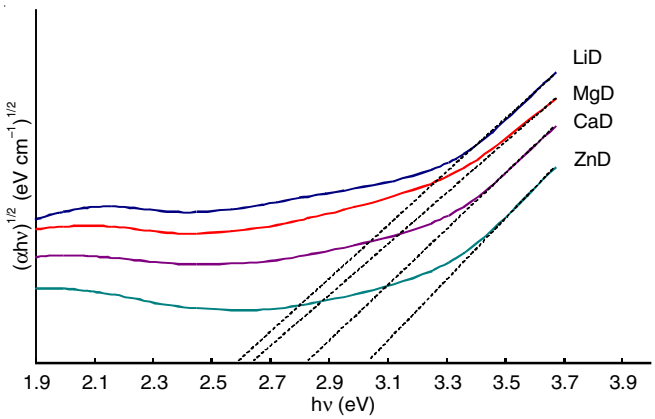

Fig. 2. Tauc plots for evaluating optical band gap of B_2O_3–SiO_2–Na_2O–CuO:MO glasses

Among different glasses, the glass mixed with 20% Li_2O boro silicate doped glass system exhibited the lowest optical band gap due to formation of NBOs [43]. As the concentration

of non-bridging oxygens increases, the network bonds become weaker and the absorption edge shifts toward longer wavelength. Fig. 3 shows a considerable increase in E_o for all glasses under study after immersion in SBF with respect to those of pre-immersed samples and are responsible for some structural changes on glass surfaces. A decrease in the optical band gap from 2.97 to 2.61 eV observed due to the successive replacement of modifier oxide ZnO by CaO, MgO and Li_2O in CuO doped soda borosilicate glass system suggests higher degree of disorder in Li_2O mixed glass (Table-4). A change in the band gap value due to immersion is found to be the highest for the glass LiD.

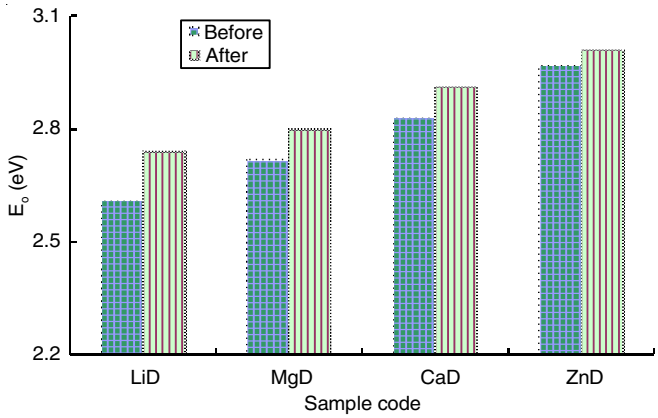

Fig. 3. The optical band gap of B_2O_3–SiO_2–Na_2O–CuO:MO glasses before and after immersion in SBF for 30 days

TABLE-4
VARIATIONS OF BAND GAPS OF PRE-SOAKED AND POST-SOAKED SAMPLES IN SBF

Sample	E_0 before immersion (eV)	E_0 after immersion (eV)
LiD	2.61	2.74
MgD	2.72	2.80
CaD	2.83	2.91
ZnD	2.97	3.01

FTIR studies: The infrared spectra of the glasses can be recorded directly in absorption/transmitted/reflected modes. In present study, we have adopted transmission mode. The impact of addition of modifier oxide on the structure of the borate network could be well understood from the fingerprint region (1600-500 cm^{-1}) where in vibrations of the boron oxygen units are active. IR spectrum of B_2O_3 containing glass in general consist three distinct active regions namely (i) symmetric stretching vibrations in the range 1200-800 cm^{-1} are due to tetrahedral borate (BO_4) units such as diborate, triborate, tetraborate and pentaborate; (ii) B-O stretching vibrations in the range 1600-1200 cm^{-1} due to trigonal borate (BO_3) units such as metaborate chains and rings, pyroborate and orthoborate and (iii) vibrations of B-O-B linkage in borate networks around 700 cm^{-1}. The details of other various IR band positions in the studied glasses are presented in Table-5. Fig. 4 represents the transmittance spectra of the glass system B_2O_3-SiO_2-Na_2O-CuO:MO recorded before immersion in SBF solution.

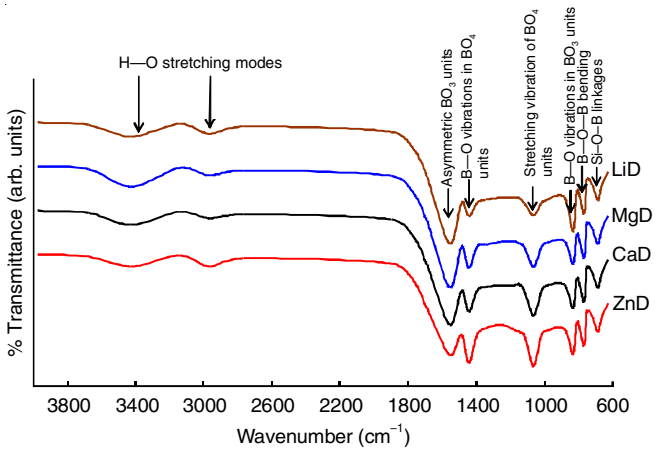

Fig. 4. FTIR spectra of glasses B_2O_3–SiO_2–Na_2O–CuO:MO before immersion in SBF solution. (The spectra are Y-shifted for the sake of clarity)

Fig. 5 presents the FTIR spectra of samples soaked in SBF solution for 30 days. The spectra of all the glasses revealed the vibrational bands phosphate and carbonate structural groups. IR spectra of Li_2O mixed glass before and after immersion along with the standard spectrum of hydroxy-apatite (HAp) layer is shown in Fig. 6. PO_4^{3-} groups show a sharp band at 430 cm^{-1} and are associated with the ν_2 double degenerated bending mode. The bands at 505 and 603 cm^{-1} are the characteristic of ν_4 of P–O–P bending and stretching vibration modes. Further, the superimposed band found at 1020 cm^{-1} is linked to the ν_3 vibration mode of the functional group Si–O–Si asymmetry/BO_4/PO_4^{3-} units. The bands in the region 1500 and 1400 cm^{-1} are due to the asymmetric stretching vibrations of carbonate group (CO_3^{2-}). The band around 1640 cm^{-1} is correlated to the H–O–H stretching, the broad bands at about 2890, 3450 cm^{-1} are linked to different modes of water band, O–H stretching or silanol groups. These specific peaks ascertain the existence of a crystalline process credited to apatite.

Weight loss studies: Weight loss of the glass samples shown in Fig. 7a reveals the chemical durability, a rise in the percentage of weight loss in lithium glass is observed. This change in weight loss is due to the transfer of the ions between the glass sample and the solution; such transfer of ions causes a change in the pH value of the residual solution yielding new stable phases. The weight loss of the studied glass samples exhibited the follows the trend LiD > MgD > CaD > ZnD.

TABLE-5
OBSERVED FTIR PEAKS AND THEIR ASSIGNMENT

Peak position (cm^{-1})	Assignment
B–O–B bending 700–690	Oxygen bridges between borons with 3- to 4-fold coordination or oxygen bridges between two borons with 3-fold coordination
BO_4 stretching 900–850	tri-, penta- and diborate groups vibrations
BO_3 stretching 1250 and 1460–1400	B–O bond stretching of trigonal units
690	Si–O–B linkage

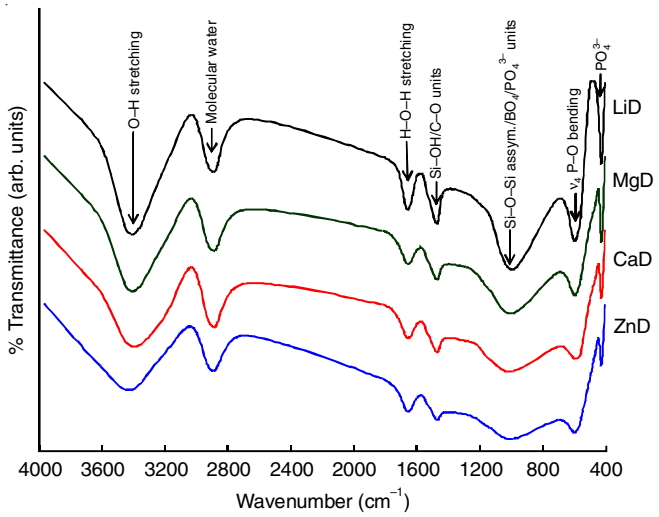

Fig. 5. FTIR transmission spectra of B_2O_3–SiO_2–Na_2O–CuO:MO glasses soaked in SBF solution for 30 days

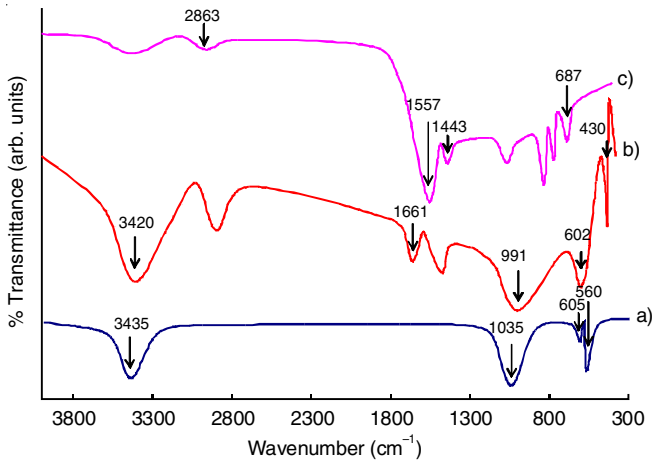

Fig. 6. Comparative FTIR spectra showing variations in LiD mixed B_2O_3–SiO_2–Na_2O–CuO:MO glass (a) HA reference (b) after 30 days of immersion (c) before immersion

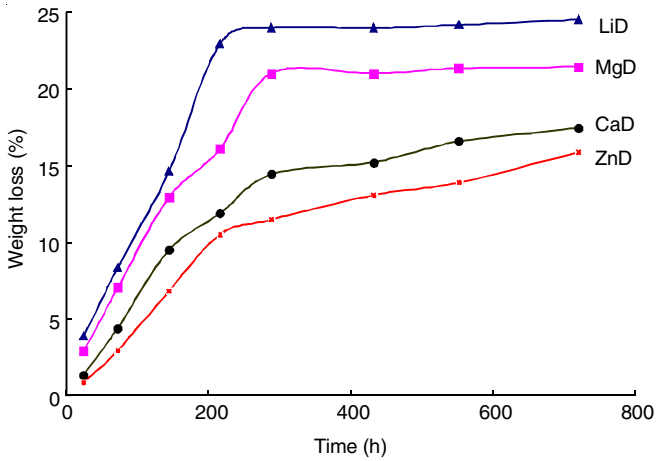

Fig. 7a. Percentage of weight loss *vs.* dissolution time of B_2O_3–SiO_2–Na_2O–CuO: MO glasses during degradation in SBF solution at 37 °C

Glass samples containing lithium oxide exhibited a higher bioactive reaction than other samples. Higher charge intensity of the Li^+ ions seem to support the full breakup of the borate network into isolated groups and facilitate the formation of apatite structure. Biological apatite constitutes the inorganic mineral phase; in normal calcified tissues the phase consists of carbonated hydroxyapatite ($Ca_{10}(PO_4)_6(OH)_2$:HA). It is the primary structural component of bones and teeth and used as a medical compound for the prevention and treatment of osteoporosis. As its formula suggests, it consists of carbonates of Ca^{2+} ions surrounded by phosphates PO_4^{2-} and hydroxides OH^-, which are usually insoluble in solution. The apatite may also be represented as $Ca_5(PO_4)_3X$, where X = OH^-, F^- or Cl^- (hydroxylapatite, fluorapatite and chlorapatite) which are bone mineral crystals and actively communicate with body fluids through the apatite channel.

pH effect: The observed high pH value of the residual SBF (in which CuO-Li_2O glass is immersed) is due to the breaking up of bridging oxygen bonds because of intensive reaction. It forms non-bridging oxygens, which disrupts networks of the glass. The high polarizing nature of non-bridging oxygens decreases the optical transmission in the UV range. Na^+ ions are more easily leached out as Na-O bonds are weaker than B–O bonds due to intense ionic character than Na^+ ions under chemical attack. Glass composition and the time of chemical attack are the other significant factors that have to be considered in addition to the influence of the pH on the chemical durability of glasses.

The pH triggering is another appropriate method for crafting smart bioactive surfaces. Fig. 7b shows the pH shift after sampling in SBF over different periods of time. A pH change may affect the ability of the cells to adhere on the surface. The pH values of SBF solution measured after 24, 72 h (and an interval of every 72 h thereafter) are found to rise sharply during first three days. It was also observed that Li_2O and MgO added glasses, the pH rises from 7.4 to 8.87 and 7.4 to 8.2, respectively, after the immersion for 3 days. After this period, the pH increases slowly and becomes almost constant as it tended to day 30. Apatite-forming ability and bioactivity is better for Li_2O added glasses when compared to that of other glasses; this could be justified from the maximum pH of 9 after 30 days of soaking in SBF solution [44,45]. The SEM and XRD studies also supported this observation.

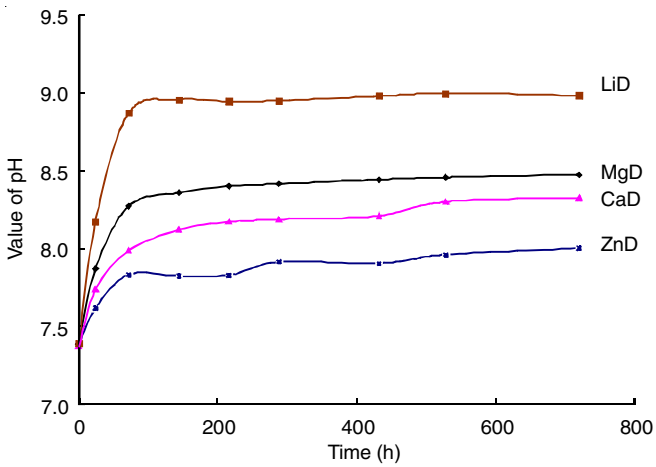

Fig. 7b. Variation of pH of SBF solution measured on various time intervals for the B_2O_3–SiO_2–Na_2O–CuO:MO glasses during immersion

In addition, the pH values of CaO doped glasses are lower compared to Li_2O and MgO, indicating a lower rate of dissolution. Among all the glasses, ZnO additive glasses shows highest durability. The pH values of the residual SBF followed the tendency $pH_{Li_2O} > pH_{MgO} > pH_{CaO} > pH_{ZnO}$.

XRD studies: Fig. 8 displays the variations in the XRD patterns of four typical glass samples. The diffractograms exhibited the diffraction peaks at 2θ = 18.43º, 31.82º, 34.15º and 46.57º due to the reflections from different planes of crystalline the HAp (JCPDS No. 09-432). The progressive development of diffraction peaks assigned to hydroxyapatite after 30 days of immersion in SBF indicates a steady increase in the hydroxyapatite crystal phase. In addition, most intense diffraction peaks due to due HAp are observed in the diffractogram of Li_2O additive glasses. In the diffractogram of MgO added glasses exhibited only two peaks at 2θ = 31.82º and 46.57º. The diffractograms have further revealed the presence of minimal quantity of hydroxyapatite in ZnO and CaO doped glasses after immersion in SBF.

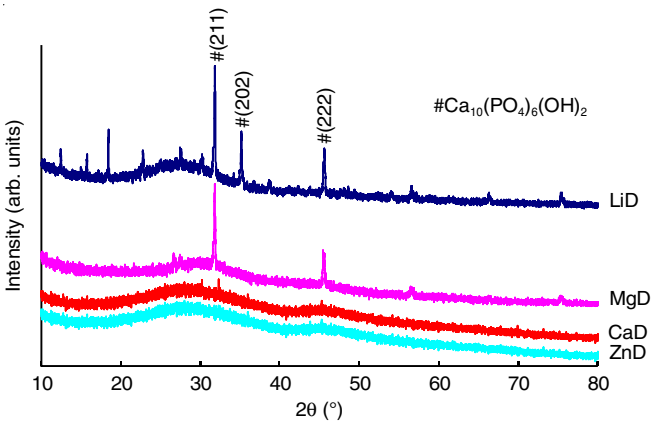

Fig. 8. XRD patterns of B_2O_3–SiO_2–Na_2O–CuO:MO glass samples after immersion in SBF for 30 days

The intensity of X-ray diffraction peak related to crystalline HA is found to the highest for LiD glass, whereas it is found to be the lowest in the diffractogram of ZnD glass. The addition of ZnO increases the overall network connectivity; this oxide participates in the glass network with ZnO_4 tetrahedral and thereby increase the resistance of the glass network against degradation. An increase in the number of topological restrictions in the glass system has shown to improve the chemical resilience of oxide glass by growing the glass network's tolerance to hydrolysis reactions. Zn^{2+} ions improve mechanical strength and chemical resistivity through the formation of tetrahedral coordination [46]. Tetrahedral ions are involved in the formation of the network and make the network of glass more rigid.

Surface morphology: Fig. 9 gives the surface morphology of soda borosilicate glasses added with different modifier oxides (Li_2O, MgO, CaO and ZnO) after soaking in SBF solution. A significant change in the mineral deposition on CuO containing sodium borosilicate bioglass samples was observed with the addition of fixed quantity (20 mol%) of various modifier oxides. The glass surfaces are clearly covered with the circular shaped flake-like apatite microcrystals. Out of four modifier oxides Li_2O shows high surface reactivity (HAp layer formation ability) than MgO, CaO and ZnO. Moreover, it is clearly visualized from the SEM micrographs that the flake-like structure decreases from LiD to ZnD, which is mainly due to decrease in degradation behaviour of the glasses in SBF. The XRD, FTIR, pH and weight loss results endorsed this inference.

EDS studies: Fig. 10 shows the energy dispersive spectra (EDS) of glass samples under study; the spectra indicated the stoichiometric proportion of all the elements present in the glass samples along with the Ca, K and P. This is an indication of the formation HAp layer over the glass samples after incubation of glasses in SBF for 30 days. Moreover, it is clearly observed from the EDS spectra that the peak intensities of calcium and phosphate are more in LiD than ZnD glass system.

Favourable energy environments such as Li^+, Na^+ attractions or ionic bonds with non-bridging oxygen (NBO) sites, which are weaker than covalent oxygen bridge bonds (BO) facilitate the diffusion of H^+ cations through the glass matrix. Exchange of Li^+, Na^+ and Ca^{2+} ions from the bioactive glass with H^+/H_3O^+ ions in the SBF solution is responsible for the increase of pH value. Presence of water bands in IR spectra that results after SBF immersion validates the cycle of ion interaction between the SBF solution and the glass surface. Existence of additive lithium oxide in the glass system speeds up the release of Li^+ and Na^+ ions from the specimen surface to the SBF solution and enhances its pH value.

Apatite layer formation is evident from the highest dissolution of Li_2O additive glass system after immersion compared to all the other glasses and the simultaneous appearance of carbonate, phosphate bands and decrease in BO_3 strength in IR spectral results. Glasses with a high dissolution degree are expected to have good antibacterial effects. Study of change in weight loss of samples is an easy method of measuring glass dissolution. Higher the glass dissolution tendency, higher the rise in local pH and alkali ion concentrations in the solution provides a stronger antibacterial effect to the glass, thus making dissolution mechanism study as essential tool to assess antibacterial effects of the glass. Consistent breakdown of the glass in the SBF solution could be seen from the curves of weight loss.

Optical studies: The optical absorption spectra indicated the presence of copper ions in Cu^{2+} and Cu^+ valence states in the glass matrix. The Cu^{2+} ions occupy octahedral positions and act as modifiers, whereas Cu^+ ions occupy tetrahedral positions in the glass network [47,48]. The optical absorption spectrum shows the highest fraction of Cu^{2+} ions that occupy octahedral positions in LiD glass compared to other three glasses, The Cu^+ ions and tetrahedral ZnO_4 units in ZnD glass form linkages with BO_4 structural units. The IR spectral studies have clearly suggested the increase in the degree of internal augmentation between various structural units as the modifier Li_2O is successively replaced by other modifier oxides, *viz.* MgO, CaO and ZnO.

Degradation studies: Lower degradability of glasses in ZnO doped glasses is observed with higher concentration of Cu^+ ions. This may be the reason for the formation of lower HAp layer content on the surface of ZnD glass when compared

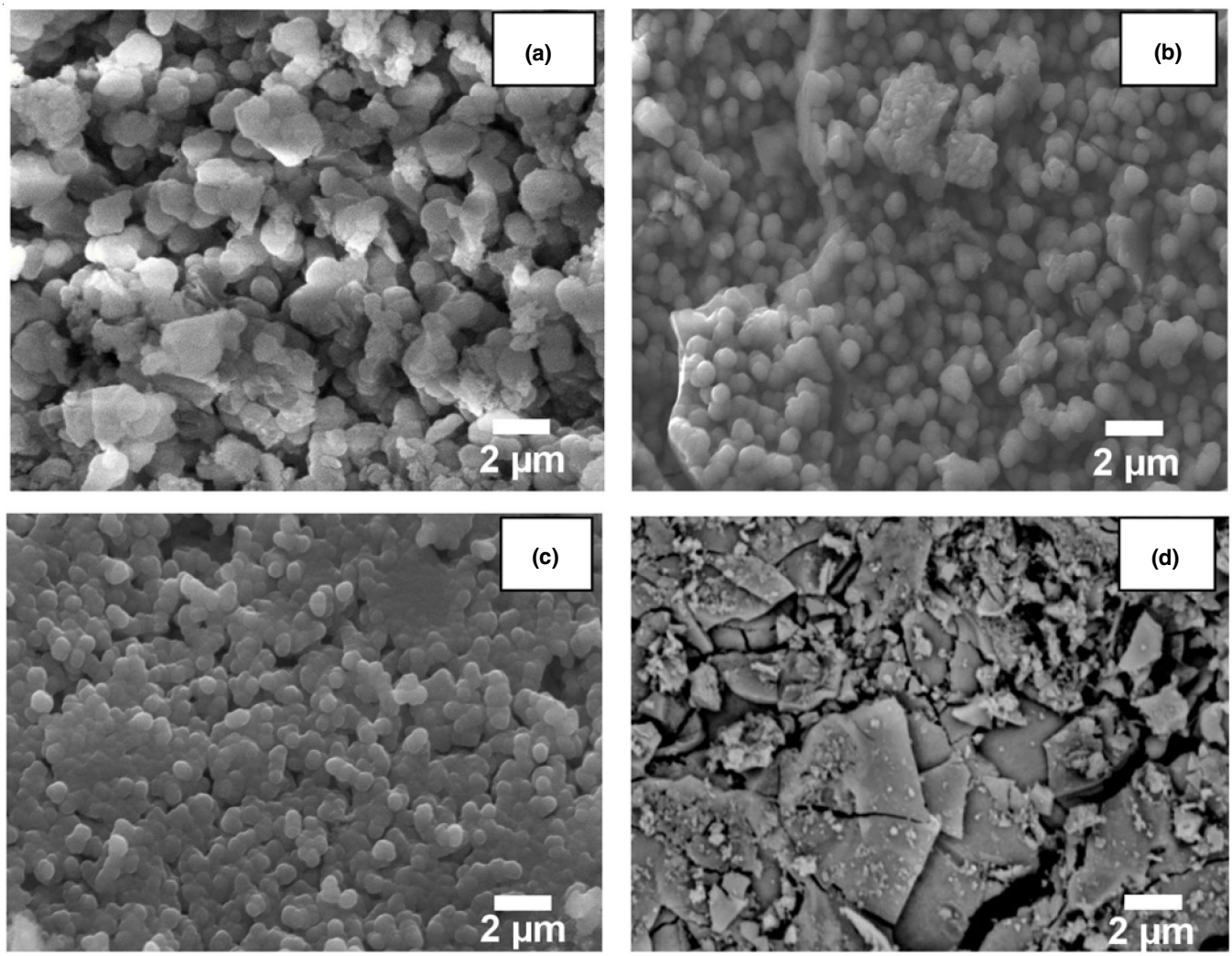

Fig. 9. SEM micrographs of B_2O_3-SiO_2-Na_2O-CuO:MO glasses after immersion in SBF solution for 30 days: (a) LiD (b) MgD (c) CaD (d) ZnD

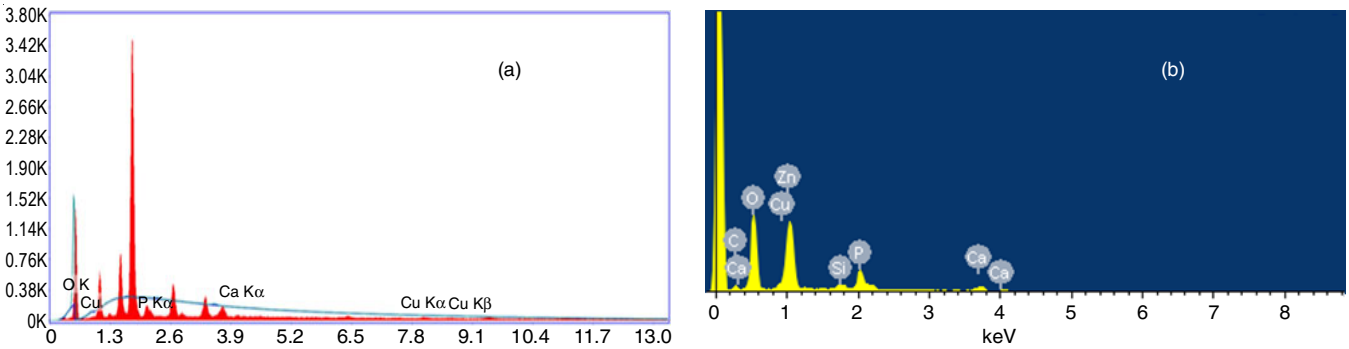

Fig. 10. Energy dispersive spectra (EDS) of glasses recorded after immersion in SBF for about 30 days: (a) LiD and (b) ZnD

with LiD. Similarly, the lower solubility of the glass is observed in CaO added glass due to the high field strength that strengthens vibration binding function. These results are fully in line with the results of weight loss and pH studies.

The dissolution of borate glasses takes place through the breakdown of the borate network where hydrolysis of B–O–B bonds is the predominant mode. Tetrahedral borate units convert back to trigonal borate groups for even higher oxide additions and the network becomes more depolymerized as the number of NBO ions increases. The smallest size of alkali ion with its high charge density has favoured the complete de-augmentation of the borate network into isolated meta, pyro, orthoborate $(BO_3)^{3-}$ type units [49]. The reactions that take place upon immersion in SBF solution, favour the formation of the hydroxyl carbonate apatite like layer on the surface of all samples and make them promising candidates for biomedical applications.

Conclusion

Analysis of the results of degradation studies showed that Li_2O has a slightly stronger impact in the rise of pH in equal amounts of CaO, MgO and ZnO replacement. The optical absorption studies showed the presence of Cu^+ and Cu^{2+} ions concurrently in samples. The remarkable difference in band gap energy is more in Li_2O glass system indicates an increase in the concentration of non-bridging oxygen (NBO) ions in the glass network leading to increased bioactivity of the material. The analysis of the results show that Li_2O is the efficient modifier to boost the bioactive properties of the glass with 0.5 mol% of CuO. The spectral analysis of XRD, SEM and IR results on the post-immersed specimens clearly showed the presence of crystalline hydroxyapatite (HAp) coating on the glass sample sheet. The quantum of the HAp coating relies heavily on the modifier in the glass matrix. The results also revealed that the replacement of 20 mol% modifier oxides *i.e.* the alkali, alkaline earth oxide and transition metal oxide in glass matrix causes inhibition of bioactivity in the following order $Li_2O < MgO < CaO < ZnO$, respectively. Hence, the Li_2O mixed glasses seems to be more suitable as an antibacterial CuO doped bioactive glass.

ACKNOWLEDGEMENTS

The authors G. Sahaya Baskaran and Y. Sudhakar thank Department of Science and Technology (DST), Government of India for providing the financial assistance to their parent institution Andhra Loyola College, Vijayawada, India, through the FIST programme.

CONFLICT OF INTEREST

The authors declare that there is no conflict of interests regarding the publication of this article.

REFERENCES

1. J.H. Beattie and A. Avenell, *Nutr. Res. Rev.*, **5**, 167 (1992); https://doi.org/10.1079/NRR19920013
2. P. Habibovic and J.E. Barralet, *Acta Biomater.*, **7**, 3013 (2011); https://doi.org/10.1016/j.actbio.2011.03.027
3. A. Hoppe, V. Mouriño and A.R. Boccaccini, *Biomater. Sci.*, **1**, 254 (2013); https://doi.org/10.1039/C2BM00116K
4. A.K. Chatterjee, R. Chakraborty and T. Basu, *Nanotechnology*, **25**, 135101 (2014); https://doi.org/10.1088/0957-4484/25/13/135101
5. C. Giacomelli, M.L. Trincavelli, C. Satriano, Ö. Hansson, D. La Mendola, E. Rizzarelli and C. Martini, *Int. J. Biochem. Cell Biol.*, **60**, 185 (2015); https://doi.org/10.1016/j.biocel.2015.01.005
6. T. Tanaka, I. Kojima, T. Ohse, J.R. Ingelfinger, S. Adler, T. Fujita and M. Nangaku, *Lab. Invest.*, **85**, 1292 (2005); https://doi.org/10.1038/labinvest.3700328
7. E. Urso and M. Maffia, *J. Vasc. Res.*, **52**, 172 (2016); https://doi.org/10.1159/000438485
8. D.C. Rigiracciolo, A. Scarpelli, R. Lappano, A. Pisano, M.F. Santolla, P. De Marco, F. Cirillo, A.R. Cappello, V. Dolce, A. Belfiore, M. Maggiolini and E.M. De Francesco, *Oncotarget*, **6**, 34158 (2015); https://doi.org/10.18632/oncotarget.5779
9. G. Mavria, Y. Vercoulen, M. Yeo, H. Paterson, M. Karasarides, R. Marais, D. Bird and C.J. Marshall, *Cancer Cell*, **9**, 33 (2006); https://doi.org/10.1016/j.ccr.2005.12.021
10. S.N. Rath, A. Brandl, D. Hiller, A. Hoppe, U. Gbureck, R.E. Horch, A.R. Boccaccini and U. Kneser, *PLoS One*, **9**, e113319 (2014); https://doi.org/10.1371/journal.pone.0113319
11. M.N. Rahaman, D.E. Day, B. Sonny Bal, Q. Fu, S.B. Jung, L.F. Bonewald and A.P. Tomsia, *Acta Biomater.*, **7**, 2355 (2011); https://doi.org/10.1016/j.actbio.2011.03.016
12. Center for Drug Evaluation and Research, Information for Consumers (Drugs)-Battle of the Bugs: Fighting Antibiotic Resistance (2011).
13. A.R. Boccaccini, D.S. Brauer and L. Hupa, Bioactive Glasses: Fundamentals, Technology and Applications, Royal Society of Chemistry (2016).
14. J.S. Fernandes, P. Gentile, R.A. Pires, R.L. Reis and P.V. Hatton, *Acta Biomater.*, **59**, 2 (2017); https://doi.org/10.1016/j.actbio.2017.06.046
15. R.D. Houlsby, M. Ghajar and G.O. Chavez, *Antimicrob. Agents Chemother.*, **29**, 803 (1986); https://doi.org/10.1128/AAC.29.5.803
16. Z.A.N. Recai, I. Hubbezoglu, A.K. Ozdemir, T. Tutku, Z. Sumer and O. Alici, *Marmara Dent. J.*, **1**, 76 (2013).
17. M. Ottomeyer, A. Mohammadkah, D. Day and D. Westenberg, *Adv. Microbiol.*, **6**, 776 (2016); https://doi.org/10.4236/aim.2016.610076
18. D.E. Day, J.E. White, R.F. Brown and K.D. McMenamin, *Glass Technol.*, **44**, 75 (2003).
19. P. Narwal, M.S. Dahiya, A. Yadav, A. Hooda, A. Agarwal and S. Khasa, *Ceram. Int.*, **43**, 11132 (2017); https://doi.org/10.1016/j.ceramint.2017.05.160
20. F. Muñoz, L. Montagne, L. Pascual and A. Durán, *J. Non-Cryst. Solids*, **355**, 2571 (2009); https://doi.org/10.1016/j.jnoncrysol.2009.09.013
21. J. Ma, C.Z. Chen, D.G. Wang, Y. Jiao and J.Z. Shi, *Colloids Surf. B Biointerfaces*, **81**, 87 (2010); https://doi.org/10.1016/j.colsurfb.2010.06.022
22. M.T. Souza, M.C. Crovace, C. Schröder, H. Eckert, O. Peitl and E.D. Zanotto, *J. Non-Cryst. Solids*, **382**, 57 (2013); https://doi.org/10.1016/j.jnoncrysol.2013.10.001
23. M. Diba, F. Tapia, A.R. Boccaccini and L.A. Strobel, *Int. J. Appl. Glass Sci.*, **3**, 221 (2012); https://doi.org/10.1111/j.2041-1294.2012.00095.x
24. S.J. Watts, R.G. Hill, M.D. O'Donnell and R.V. Law, *J. Non-Cryst. Solids*, **356**, 517 (2010); https://doi.org/10.1016/j.jnoncrysol.2009.04.074
25. J.M. Oliveira, R.N. Correia, M.H. Fernandes and J. Rocha, *J. Non-Cryst. Solids*, **265**, 221 (2000); https://doi.org/10.1016/S0022-3093(99)00957-6
26. J.M. Fernández-Navarro, El vidrio, Colección Textos Universitarios no. 6, C.S.I.C, Madrid (1991).
27. M.M. Elkholy, *J. Lumin.*, **130**, 1880 (2010); https://doi.org/10.1016/j.jlumin.2010.05.002
28. S. Arabyazdi, A. Yazdanpanah, A. Ansari Hamedani, A. Ramedani and F. Moztarzadeh, *J. Non-Cryst. Solids*, **503–504**, 139 (2019); https://doi.org/10.1016/j.jnoncrysol.2018.09.040
29. G.R. Kumar, T. Srikumar, G.M. Krishna, G.S. Baskaran, A.S.S. Reddy, V.R. Kumar and Ch. Srinivasa Rao, *J. Non-Cryst. Solids*, **498**, 372 (2018); https://doi.org/10.1016/j.jnoncrysol.2018.03.025
30. M.O. Bensaid, L. Ghalouci, S. Hiadsi, F. Lakhdari, N. Benharrats and G. Vergoten, *Vib. Spectrosc.*, **74**, 20 (2014); https://doi.org/10.1016/j.vibspec.2014.07.001
31. Y.B. Saddeek and L.A.E. Latif, *Phys. B*, **348**, 475 (2004); https://doi.org/10.1016/j.physb.2004.02.001
32. B. Sumalatha, I. Omkaram, T.R. Rao and C.L. Raju, *Physica B*, **411**, 99 (2013); https://doi.org/10.1016/j.physb.2012.11.021
33. T. Du and O.J. Ilegbusi, *J. Mater. Sci.*, **39**, 6105 (2004); https://doi.org/10.1023/B:JMSC.0000041712.35581.4c
34. M.J. Klink and A.M. Crouch, *Mikrochim. Acta*, **166**, 27 (2009); https://doi.org/10.1007/s00604-009-0157-z
35. R. Stefan, E. Culea and P. Pascuta, *J. Non-Cryst. Solids*, **358**, 839 (2012); https://doi.org/10.1016/j.jnoncrysol.2011.12.079
36. T.R. Rao, C.V. Reddy, C.R. Krishna, U.S.U. Thampy, R.R. Raju, P.S. Rao and R.V.S.S.N. Ravikumar, *J. Non-Cryst. Solids*, **357**, 3373 (2011); https://doi.org/10.1016/j.jnoncrysol.2011.06.004
37. G.J. Mohini, N. Krishnamacharyulu, G. Sahaya Baskaran, P.V. Rao and N. Veeraiah, *Appl. Surf. Sci.*, **287**, 46 (2013); https://doi.org/10.1016/j.apsusc.2013.09.055

38. G. Jagan Mohini, G. Sahaya Baskaran, V. Ravi Kumar, M. Piasecki and N. Veeraiah, *Mater. Sci. Eng. C*, **57**, 240 (2015); https://doi.org/10.1016/j.msec.2015.07.048
39. N. Krishnamacharyulu, G.J. Mohini, G.S. Baskaran, V.R. Kumar and N. Veeraiah, *J. Non-Cryst. Solids*, **452**, 23 (2016); https://doi.org/10.1016/j.jnoncrysol.2016.07.044
40. A. Oyane, H.M. Kim, T. Furuya, T. Kokubo, T. Miyazaki and T. Nakamura, *J. Biomed. Mater. Res.*, **65A**, 188 (2003); https://doi.org/10.1002/jbm.a.10482
41. A. Edukondalu, B. Kavitha, M.A. Samee, S. Kareem Ahmmed, S. Rahman and K. Siva Kumar, *J. Alloys Compd.*, **552**, 157 (2013); https://doi.org/10.1016/j.jallcom.2012.10.010
42. K.N. Kumar, B. Suresh, A. Ingram, M. Kostrzewa, P. Bragiel, V.R. Kumar and N. Veeraiah, *Ceram. Int.*, **43**, 6385 (2017); https://doi.org/10.1016/j.ceramint.2017.02.049
43. N. Rezlescu, E. Rezlescu, I. Ciobotaru, M.L. Craus and P.D. Popa, *Ceram. Int.*, **24**, 31 (1998); https://doi.org/10.1016/S0272-8842(96)00073-9
44. V. Miguez-Pacheco, T. Buttner, A.L.B. Macon, J.R. Jones, T. Fey, D. de Ligny, P. Greil, J. Chevalier, A. Malchere and A.R. Boccaccini, *J. Non-Cryst. Solids*, **432**, 65 (2016); https://doi.org/10.1016/j.jnoncrysol.2015.03.027
45. T. Srikumar, I.V. Kityk, Ch. Srinivasa Rao, Y. Gandhi, M. Piasecki, P. Bragiel, V. Ravi Kumar and N. Veeraiah, *Ceram. Int.*, **37**, 2763 (2011); https://doi.org/10.1016/j.ceramint.2011.04.031
46. D. Rajeswara Rao, G. Sahaya Baskaran, V. Ravi Kumar and N. Veeraiah, *J. Non-Cryst. Solids*, **378**, 265 (2013); https://doi.org/10.1016/j.jnoncrysol.2013.07.001
47. A. Thulasiramudu and S. Buddhudu, *Spectrosc. Radiat. Transf.*, **97**, 181 (2006); https://doi.org/10.1016/j.jqsrt.2005.04.006
48. L.S. Rao, M.S. Reddy, D.K. Rao and N. Veeraiah, *Solid State Sci.*, **11**, 578 (2009); https://doi.org/10.1016/j.solidstatesciences.2008.06.022
49. Y. Sudhakar, G. Sahaya Baskaran, V. Ravi Kumar, G. Little Flower and B. Deva Prasad Raju, *Opt. Mater.*, **98**, 109451 (2019); https://doi.org/10.1016/j.optmat.2019.109451